ChemInform Abstract: Activation of 1.54 µm Er3+ Fluorescence in Concentrated II–VI Semiconductor Cluster Environments

ARTICLE *in* CHEMINFORM · APRIL 2010

Impact Factor: 0.74 · DOI: 10.1002/chin.199815008

Activation of 1.54 μm Er^{3+} Fluorescence in Concentrated II−VI Semiconductor Cluster Environments

Thomas Schmidt, Gerd Müller, and Lubomir Spanhel*

Lehrstuhl für Silicatchemie in der Fakultät für Chemie und Pharmazie, Universität Würzburg, Röntgenring 10, 97070 Würzburg, Germany

Klaus Kerkel and Alfred Forchel

Technische Physik, Universität Würzburg, Am Hubland, 97074 Würzburg, Germany

Received April 14, 1997. Revised Manuscript Received November 11, 1997

A strong enhancement of the 1.54 μm fluorescence of Er^{3+} has been achieved in highly concentrated II−VI semiconductor quantum dot environments. A new preparation strategy allowed to incorporate up to 20 at. % Er^{3+} into ZnS, CdS, and CdSe as well as ZnO semiconductor clusters and nanocrystals (sizes 1.5−5 nm). All clusters investigated contain OH groups that serve as bridging ligands for the lanthanide attachment. Er^{3+} in ethanolic cluster solutions is fluorescing by 3 orders of magnitude more strongly than in pure ethanol, which can only be explained by a cagelike architecture of these clusters offering a large intake capacity. With this new material concept, the two well-known radiationless recombination channels related to electron−phonon coupling and Er−O−Er clustering can be controlled. First, with decreasing number of erbium ions per nanoparticle, the fluorescence intensity increases, approaching its maximum at 2 at. % Er^{3+}. Second, it is shown that the fluorescence intensity increases with decreasing energy of phonons produced by lattice vibrations of the surrounding cluster carrier. For example, ethanolic molecular erbium/(aminopropyl)trialkoxysilane (AMEO) complexes exhibit the lowest fluorescence intensity of all samples employed, due to the presence of high-energy OH and NH vibrations (between 3000 and 3500 cm^{-1}). Ethanolic Er/ZnO colloids, however, fluoresce 100 times more intense, which can be interpreted in terms of the lower phonon energy of the ZnO lattice vibrations (between 500 and 1000 cm^{-1}). The AMEO-capped 1.6 nm CdSe/Er^{3+} clusters in ethanol fluoresce 1000 times more strongly than ethanolic AMEO/Er^{3+} complexes (CdSe phonon energies around 200 cm^{-1}).

Introduction

The initiation of small semiconductor and metal particle research related to the development of novel materials for photocatalysis, solar energy storage, and size tunable linear and nonlinear optics goes back to the beginning 1980s and is summarized in several review articles and books.[1−9] Since the early 1990s, structure and application oriented work on semiconductor quantum dots (QD) is increasing due to improved synthesis routes. They allow preparing highly concentrated colloidal cluster solutions for the growth of large crystals[10−12] and for film preparations.[13−15]

In this paper, we present a semiconductor quantum dot approach to control NIR fluorescence of Er^{3+}. Silicate glass fibers doped with erbium ions are important NIR laser components used for the light signal recovery in telecommunication networks.[16] Promising complementary components for optical signal processing might also be represented by short distance planar waveguides.[17] To increase the NIR laser efficiency (by lowering the phonon energy of the matrix) and to shorten the pumping distance (by introducing high content of homogeneously distributed Er^{3+}), new material compositions and fabrication technologies are required. Heavy metal fluoride, oxide, and chalcogenide glasses are known to exhibit lower phonon energies

* Corresponding author. E-mail: spanhel@silchem.uni-wuerzburg.de.

(1) Henglein, A. *Chem. Rev. (Washington, D.C.)* **1989**, *89*, 1861.
(2) Grätzel, M. *Heterogeneous Photochemical Electron Transfer*; CRC: Boca Raton, FL, 1989.
(3) Brus, L. *Appl. Phys. A* **1991**, *53*, 463.
(4) Wang, Y. *Acc. Chem. Res* **1991**, *24*, 133; *Adv. Photochem.* **1995**, *19*, 179.
(5) Gleiter, H. *Phase Transitions* **1990**, *24−26*, 15.
(6) Flytzanis, C.; Hache, F.; Klein, M. C.; Ricard, D.; Roussignol, Ph. *Prog. Opt.* **1991**, *29*, 323.
(7) Weller, H. *Adv. Mater.* **1993**, *5* (2), 88.
(8) Schmid, G. *Clusters and Colloids*; VCH: Weinheim, 1994.
(9) Woggon, U.; Gaponenko, S. V. *Phys. Status Solidi B* **1995**, *189*, 285.
(10) Spanhel, L.; Anderson, M. A. *J. Am. Chem. Soc.* **1990**, *112*, 2279; **1991**, *113*, 2826.
(11) Vossmeyer, T.; Reck, G.; Katsikas, L.; Haupt, E.; Schulz, B.; Weller, H. *Science* **1995**, *267*, 1476.
(12) Murray, C. B.; Kagan, C. R.; Bawendi, M. G. *Science* **1995**, *270*, 1335.
(13) Anderson, M.; Gieselmann, M. J.; Xu, Q. *J. Membr. Sci.* **1988**, *39*, 243.
(14) O'Regan, B.; Moser, J.; Anderson, M.; Grätzel, M. *J. Phys. Chem.* **1990**, *94*, 8720.
(15) Spanhel, L. *E-MRS Monogr.* 1**992**, *5*, 407.
(16) Chenard, F. *Photonics Spectra*; Special CLEO Issue on Rare-Earth-Doped Fibers, 1994; p 126.
(17) Kitagawa, T.; Bilodeau, F.; Malo, B.; Theriault, S.; Albert, J.; Jihnson, D. C.; Hill, K. O.; Hattori, K.; Hibino, Y. *Electron. Lett.* **1994**, *30* (16), 1311.

S0897-4756(97)00216-0 CCC: $15.00
Published on Web 01/19/1998

which reduce the extent of electron−phonon interaction and improve the laser performance.[18] On the other hand, high Er^{3+} contents of up to 15 at. % were already demonstrated on sol−gel-derived materials such as silicates,[19] alumosilicates,[20] TiO_2,[21] and GeO_2[22] as well as organosilicates filled with nanocrystalline ZnO carriers.[23]

In this contribution, we present the synthesis of colloidal Er^{3+}-containing II−VI quantum crystallites for planar waveguide formation. This preliminary study was directed toward following three goals: (1) to activate the 1.54 μm fluorescence by attaching Er^{3+} to the II−VI quantum dot, (2) to study the influence of the chemical composition of the semiconductor clusters on the 1.54 μm fluorescence intensity of Er^{3+}, and (3) to synthesize highly concentrated metal chalcogenide and oxide nanocolloids with high Er^{3+} content and to employ them in the preparation of thick films via single step coating.

Experimental Section

Materials. All manipulations involving silylchalcogenides were carried out under argon using the Schlenk technique. Cadmium and zinc acetate dihydrates were purchased from Fluka. Bis(trimethylsilyl)selenium, $(TMS)_2Se$, was prepared according to the procedure described elsewhere[24] and stored at −30 °C under argon. Bis(trimethylsilyl) sulfide, $(TMS)_2S$, and ethanol from Aldrich were used as purchased. 3-(Aminopropyl)triethoxysilane (AMEO) was purchased from ABCR.

Synthesis of Cd/Er and Zn/Er Precursors for Chalcogenolysis. A 2.3 g sample of dehydrated cadmium acetate (or 1.83 g of zinc acetate) together with the desired amount of erbium acetate (atomic Cd/Er or Zn/Er ratios ranging between 5 and 20) were suspended in 100 mL of ethanol. The metal acetate mixture dissolved during refluxing for 3 h. Finally, the solvent was removed under reduced pressure and ambient temperature, yielding crystalline powders.

Chalcogenolysis of Er/Cd(Zn)E (E = S, Se) Precursors. The nanocolloids were synthesized according to the following general procedure: Cd/Er or Zn/Er precursor powder was dissolved in ethanol and reacted with (aminopropyl)triethoxysilane (AMEO) to yield a 0.2 M Cd complex with the AMEO/Cd(Zn) ratio of 5. The reagent, placed in a two-neck flask, was thoroughly deoxygenated by repeated evacuation and flushing with argon. The synthesis of a concentrated metal chalcogenide cluster solutions was completed by dropwise addition of the liquid bis(trimethylsilyl)selenium or -sulfur source. The resulting erbium-containing metal chalcogenide colloidal solutions were approximately 0.1−0.5 M (with respect to chalcogenium atom) and contained 100% mole excess of cadmium or zinc.

Using the spin on technique, optically transparent films on glass substrates or on Si wafers were prepared from the 0.1 M or subsequently concentrated 0.5 M colloids. The thermal curing of these films was performed under vacuum conditions at 100 °C for 2 h. The average thickness of the resulting crack-free films can be adjusted between 2 and 10 μm per single step coating.

Synthesis of Er^{3+}/ZnO Coating Sols and Nanocrystalline Films. Two routes were developed to prepare highly concentrated stable Er^{3+}/ZnO nanocolloids containing hexagonal wurtzite crystallites with sizes around 3.5 and 5 nm as checked by XRD.

Route A, 3.5 nm Particles. An ethanolic suspension of a mixture of dehydrated zinc and erbium acetate was refluxed for 3 h under ambient air conditions, and the resulting clear pink 0.1 M Zn−O−Er precursor solution was cooled to room temperature. For this procedure, the Zn/Er ratios ranging between 2 and 40 were adjusted by varying the Zn content whereas the Er concentration remained constant. The hydrolysis and condensation yielding 3.5 nm ZnO clusters was induced by dropwise addition of tetramethylammonium hydroxide, TMAH (2.2 M stock solution in methanol), the TMAH/Zn ratio being one. Subsequent concentrating on a rotary evaporator (10 Torr, 30 °C) yielded stable 2 M ZnO/Er colloids. Assuming spherical geometry, it was calculated that 3.5 nm nanocrystals contain 950 ZnO molecules with approximately 300 being situated on the surface. The mean particle distance was calculated to be about one particle diameter.

Route B, 5 nm Particles. This route, developed for the preparation of thick electronically conducting nanocrystalline Al/ZnO films,[25] employs 80 mL of a 1-propanolic 0.5 M zinc acetate dihydrate suspension. After heating to 125 °C and refluxing for 20 min, 18 mL of a 2.2 M methanolic TMAH solution was rapidly added. Subsequently, the hot solution was cooled to 40 °C, yielding a nearly neutral (pH = 8) 0.4 M ZnO colloid. Subsequent concentrating on a rotary evaporator under vacuum conditions (10 Torr) gave 20 mL of a 2 M ZnO colloid. In the final step and under stirring, dehydrated erbium acetate powder was added to the 2 M ZnO solution. Erbium acetate powder is soluble neither in ethanol nor in 1-propanol, but it readily dissolves within a few minutes in this concentrated ZnO colloid up to a molarity of about 0.4 M Er^{3+} (Zn/Er ratio = 5). Several other lanthanide acetates, which are not soluble in 1-propanol, are highly soluble in 2 M ZnO colloids, too. In these colloids the agglomeration number was calculated to be 2750 ZnO molecules per particle with 950 of them being situated on the surface. The mean particle distance was calculated to be approximately 1.2 particle diameter.

The 2 M ZnO/Er colloids were further used to prepare films on commercial glass slides by dip coating. The apparatus used was equipped with a sintering oven and allows coating under controlled humidity and withdrawal speed (2−70 cm/min). It also allows to transfer the wet films from the coating chamber into the oven chamber without exposing them to the ambient air. The rapid sintering of the films (by transferring the wet films into the preheated oven) was performed under dry air stream conditions for 2 h. The sintering temperature ranged between 250 and 400 °C. The largest film thickness per single step coating achieved was 1.5 μm as determined on sintered crack-free optically transparent films.

Optical Characterization. Optical absorption spectra were collected with a Perkin-Elmer Lambda 19 spectrophotometer. Quartz cells with thickness ranging between 10 μm and 1 cm were used to obtain spectra from concentrated colloids.

NIR Fluorescence Measurements. The room-temperature steady-state NIR spectra of erbium-containing samples were taken using a chopped 200 mW CW Ar^+ laser (chopper frequency was 36 Hz) and a liquid nitrogen cooled Ge detector. The 488 nm pump wavelength was chosen to induce the $^4I_{15/2} \rightarrow {}^4F_{7/2}$ transition (=20 492 cm^{-1}) in Er^{3+}. The detection range was between 1400 and 1700 nm.

(18) Reisfeld, R.; Jorgensen, Ch. K. In *Handbook on the Physics and Chemistry of Rare Earths*; Gschneidner, K. A. , Jr., Eyring, L., Eds.; Elsevier: Amsterdam, 1987 and references therein.
(19) Sun, K.; Lee, W. H.; Risen, W. M. *J. Non-Cryst. Solids* **1987**, *92*, 145.
(20) Wu, F.; Puc, G.; Foy, P.; Snitzer, E.; Sigel, G. H. *Mater. Res. Bull.* **1993**, *28*, 637.
(21) Bahtat, A.; Bouazaoui, M.; Bahtat, M.; Mugnier, J. *Opt. Commun.* **1994**, *111*, 55.
(22) Yamazaki, M.; Kojima, K. *J. Mater. Sci. Lett.* **1995**, *14*, 813.
(23) Spanhel, L.; Popall, M.; Müller, G. *Proc. Indian Acad. Sci. (Chem. Sci.)* **1995**, *107*, 637.
(24) Schmidt, M.; Ruf, H. *Z. Anorg. Allg. Chem.* **1963**, *321*, 270.
(25) Hilgendorff, M.; Spanhel, L.; Müller, G., submitted to *J. Electrochem. Soc.*
(26) Jorgensen, C. K.; Judd, B. R. *Mol. Phys.* **1964**, *8*, 281.
(27) Yatsimirski, K. B.; Davidenko, N. K. *Coord. Chem. Rev.* **1979**, *27*, 223.
(28) Ratnakaram, Y. C. *Phys. Chem. Glasses* **1994**, *35*, 182.
(29) Kamat, P. V.; Patrick, B. *J. Phys. Chem.* **1992**, *96*, 6830.

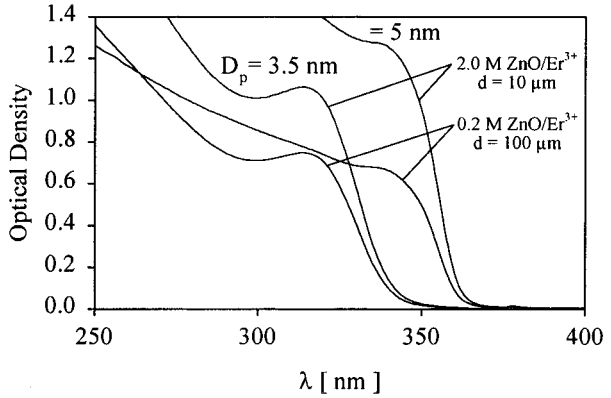

Figure 1. Optical absorption spectra of alcoholic 0.2 and 2 M ZnO colloids for two different particle sizes. All samples contain 20 at. % Er^{3+}.

Results and Discussion

Optical Absorption Properties of Er^{3+}/ZnO Colloids. Figure 1 shows optical absorption spectra of highly concentrated differently sized ZnO/Er colloids taken with 10 and 100 μm quartz cells (ZnO/Er = 5). The excitonic transitions at 320 nm indicate the presence of strongly quantized 3.5 nm particles. The 350 nm transitions correspond to sizes of about 5 nm (also confirmed in TEM measurements), in contrast to large ZnO bulk crystals which have an absorption band edge at 400 nm. The spectra in Figure 1 also show a nonlinear ZnO concentration dependency of the optical density. Below concentrations of 0.1 M, the sols obey the Lambert−Beer law ($\epsilon_{320} = 500\ M^{-1}\ cm^{-1}$, $\epsilon_{350} = 250\ M^{-1}\ cm^{-1}$). Above 0.1 M, the optical densities rise with increasing ZnO concentration. Surprisingly, the presence of erbium ions in all investigated colloids did not influence the growth of ZnO nanocrystals, neither their optical absorption spectra nor the XRD and TEM patterns.[36] The cluster size dependent energy position and shape of the excitonic transitions shown in Figure 1 coincide with spectroscopic observations made on erbium-free colloids and with earlier studies.[10,29]

Optical absorption spectra of the above colloids taken with 1 cm cells are depicted in Figure 2. It shows the optical absorption edge of the ZnO particles located below 400 nm along with the characteristic weak Er^{3+} transitions between 360 and 1000 nm (parity-forbidden). For comparison, spectra of an aqueous erbium acetate and an ethanolic Er−O−Zn precursor solution are also included. Environment-related differences in shape and intensity of the $^4G_{11/2}$ and $^2H_{11/2}$ transitions at 377 and 520 nm can be recognized in the Er^{3+} spectra (Figure 2).

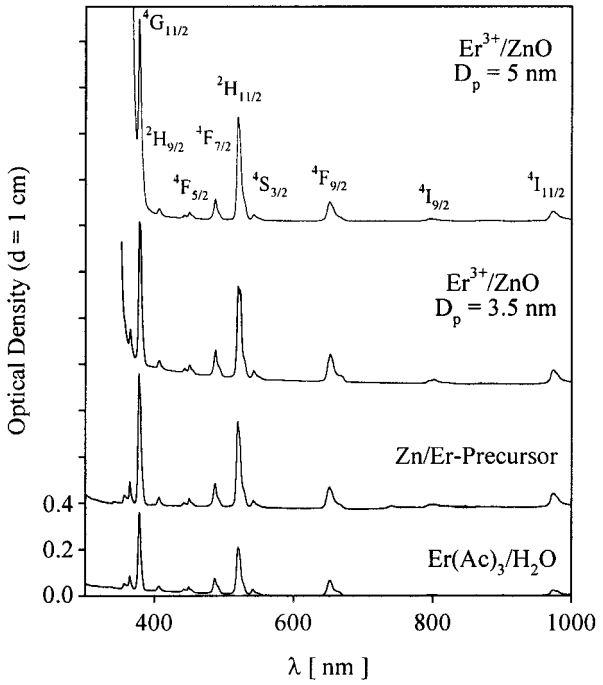

Figure 2. Optical absorption spectra of erbium ions in water, in an ethanolic Zn−O−Er precursor before hydrolysis, and in two alcoholic ZnO colloids of different particle size. The molar concentration of erbium was 0.05 M in all four liquid samples (Zn/Er = 5). Note the hyperchromic term splitting of the two $^4G_{11/2}$ and $^2H_{11/2}$ transitions.

From the literature,[18,26−28] it is well-known that these two $^4G_{11/2}$ and $^2H_{11/2}$ transitions (and transitions of other lanthanides in different ligand fields) are hypersensitive pseudoquadrupolar, which is reflected in nephelauxetic band shifts, ligand field induced term splitting, and an increase in the oscillator strength. These changes, observed in experimental studies on glasses and liquid complexes as well as in theoretical Judd−Ofelt and Jorgensen calculations,[18,26−28] are explained in terms of variable ligand−metal orbital overlap due to different point symmetries and electronegativities of the ligands.

In our colloid study, nephelauxetic $^2H_{11/2}$ band shifts were not detected, and a more detailed examination of this transition revealed a significant band broadening and hyperchromic effect in all investigated Er/ZnO colloids. This is illustrated in detail in Figure 3 showing the $^2H_{11/2}$ band of an aqueous erbium acetate complex compared to the spectra of differently sized colloids. The left-hand spectra indicate that the heterometallic Er−O−Zn precursor cluster[30] as well as the subsequently prepared colloids exhibits comparable hyperchromic band broadening. Large ZnO/Er ratios in these colloids cause the transformation of a shoulder at 522 nm into a peak after the condensation process (Figure 3, left).

The right-hand side of Figure 3 also displays hyperchromic band broadening detected after dissolving erbium acetate in neutral 1-propanolic ZnO colloids, indicating deposition of liberated Er^{3+} onto ZnO particles. The molar extinction coefficient of about 8 $M^{-1}\ cm^{-1}$ was found to be comparable with that of the co-condensed ZnO/Er sols from route A. At ZnO/Er ratios ≥ 20, the maximum value of about 11 $M^{-1}\ cm^{-1}$ was

(30) For the following discussion it is more realistic to use the term of cluster, rather than to think of monomeric molecular precursors. For example, already the dehydrated zinc acetate employed in this study is known to be not the simple $Zn(OAc)_2$ but to be the tetrahedral $Zn_4O(Ac)_6$ cluster. Acetate-capped alkoxides and heteroalkoxides of bivalent metals are known to exhibit even more complex oligomeric structures composed of up to 12 metal atoms (see for example Mehrotra, R. C. *J. Sol-Gel Sci. Technol.* **1994**, *2*, 1).

(31) Reisfeld, R.; Eckstein, Y. *J. Non-Cryst. Solids* **1973**, *12*, 357.
(32) Desurvire, E. *Erbium-Doped Fiber Amplifiers*; John Wiley & Sons: New York, 1994.
(33) Robinson, C. C. *J. Non-Cryst. Solids* **1974**, *15*, 1.
(34) Ptatschek, V.; Schmidt, T.; Lerch, M.; Müller, G.; Emmerling, A.; Fricke, J.; Foitzik, A. H.; Langer, E.; Spanhel, L. *Ber. Bunsen-Ges. Phys. Chem.*, in press.
(35) Klein, M. C.; Hache, F.; Ricard, D.; Flytzanis, C. *Phys. Rev. B* **1990**, *42*, 11123.
(36) Spanhel, L.; Schmidt, T.; Müller, G.; Mais, N.; Forchel, A. *Chem. Mater.*, to be submitted.

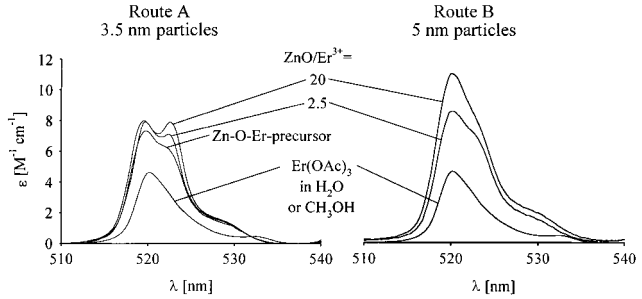

Figure 3. Spectral changes of the $^2H_{11/2}$ band in alcoholic precursor solutions and ZnO colloids for two different synthesis routes and two different atomic ZnO/Er^{3+} ratios. For comparison, the spectrum of an aqueous/methanolic erbium acetate reference solution of the same molar concentration (0.05 M) is also included (for details see text).

determined. From the area under the absorption bands on the wavenumber scale, we have determined the oscillator strength P to be 5×10^{-6} for the aqueous (or methanolic) acetate complex, which is nearly 3 times lower than the maximum P value of 13×10^{-6} calculated for the ZnO/Er colloid. The magnitude of this ZnO environment-related hypersensitivity coincides with literature reports on Er^{3+}-containing oxide glasses based on germanate ($P \times 10^6 = 11$), phosphate (=13), borate (=15.1), or zinc sulfate (=15.23).[28,31]

It would go beyond the scope of this paper to give an additional theoretical Judd−Ofelt-based Ω_2 parameter analysis of the found hypersensitivity, apparently related to stronger erbium−oxygen orbital overlap within the Zn−O-rich ligand field. Nevertheless, the above-presented experimental data indicate that both routes produce ZnO particles with surface bound erbium ions, no matter whether the erbium is present during the ZnO condensation process or added afterward. Moreover, it seems that not only in co-condensed sols but also during the erbium salt dissolution in ZnO colloids the liberated erbium ions appear to occupy the particle surface as well as the interior of the particles. This will be evaluated in the next section, where NIR fluorescence studies on Er^{3+}/ZnO are presented.

NIR Fluorescence Properties of Er^{3+}/ZnO Colloids. From NIR fluorescence studies on Er^{3+} embedded in glasses, it is known that photoexcited Er^{3+} ions emit 1.54 μm photons more efficiently if a matrix of lower phonon energy is used.[18] Due to electron−phonon interactions, the existing radiationless recombination channel conserves fluorescence. The number of phonons p (excited lattice vibrations) required to conserve the energy of the excited state in a multiphonon decay between energy levels $^4I_{13/2}$ and $^4I_{15/2}$ (the last being the ground-state level of Er^{3+}) can be calculated according to[32]

$$p = \Delta E/\hbar\omega = 6537\ \mathrm{cm}^{-1}/\hbar\omega \qquad (1)$$

where $\Delta E = 6537\ \mathrm{cm}^{-1}$ (fluorescence maximum at 1.54 μm) is the energy gap between $^4I_{13/2}$ and $^4I_{15/2}$ levels and $\hbar\omega$ is the energy of phonons (expressed in wavenumbers) of the surrounding medium. The relationship between the nonradiative multiphonon relaxation rate W_{nr} and the number of phonons p can be approximated through the relation[18]

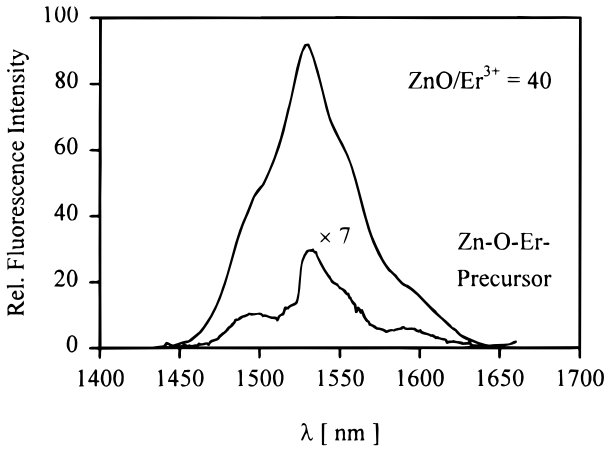

Figure 4. NIR fluorescence spectrum of an ethanolic 2 M Zn−O−Er precursor before and after the hydrolysis and ZnO condensation. Excitation conditions: pump wavelength = 488 nm of a CW Ar^+ laser; ambient laboratory conditions.

$$W_{nr} = A \exp(-Bp) \qquad (2)$$

where A (in hertz) and B are constants. Further, when this multiphonon decay is the predominant mechanism, the fluorescence quantum yield η is related to the radiative and nonradiative recombination rate W_r and W_{nr} by

$$\eta = W_r/W_r + W_{nr} \qquad (3)$$

Accordingly, with increasing number of phonons p, i.e., by lowering the vibration energy of the Er^{3+} environment (eq 1), W_{nr} decreases (eq 2), which enhances η of the 1.54 μm fluorescence (eq 3).

In alcoholic Er^{3+}/ZnO colloids, there are several kinds of vibrations deactivating the energy of the excited state of Er^{3+}, for example, the high-energy OH and CH vibrations of alcohol solvent between 3500 and 2700 wavenumbers and low-energy lattice vibrations of ZnO nanocrystals located around 500 wavenumbers.[36] Considering eqs 1 and 2, the multiphonon relaxation rate in a ZnO matrix ($\propto e^{-13}$) is by almost 5 orders of magnitude lower than in an alcohol environment ($\propto e^{-2}$) so that we might expect for Er^{3+} residing within ZnO particles to fluoresce more strongly than Er^{3+} surrounded by alcohol molecules.

Figure 4 shows the fluorescence spectra of an ethanolic Zn−O−Er precursor cluster before and after hydrolysis and condensation. After completion of condensation (development of ZnO nanocrystallites), the measured fluorescence intensity was by 2 orders of magnitude higher than before, indicating that the above-described multiphonon deexcitation should be taken into account. In addition, the relatively broad fluorescence bands, located between 1450 and 1650 nm, show five Stark levels for the precursor solution whereas four Stark levels are seen for the condensed colloid. Similarly to the hypersensitivity of the $^2H_{11/2}$ transition discussed above, the Stark splitting seen in Figure 4 is a sensitive indicator of the symmetry changes of different ligand fields. According to the literature,[32] lower numbers of Stark levels represent a higher symmetry of Er^{3+} sites in the host matrix. This implies that Er^{3+} bound to ZnO after the condensation process seems to have a different symmetry (with lower coordination

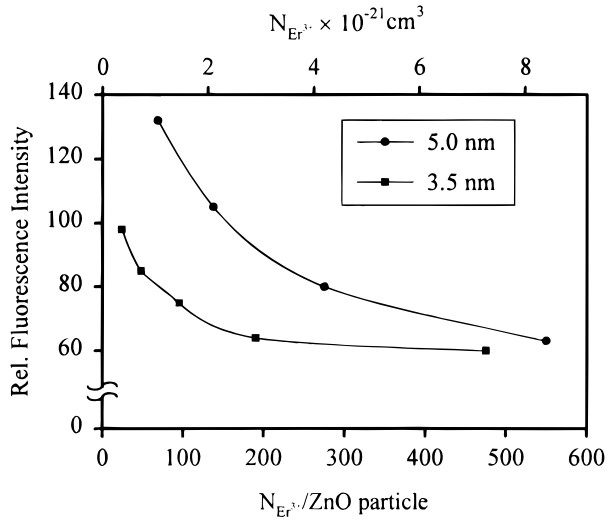

Figure 5. Intensity of the 1.54 μm fluorescence plotted against the number of erbium ions per ZnO particle for two different nanocrystal sizes and synthesis routes. Assuming spherical geometry, the agglomeration numbers are 950 (for 3.5 nm size) and 2750 (for 5 nm size) molecules per ZnO particle. The upper scale displays the corresponding erbium ion concentration per cm^3 ZnO.

number) than in the precursor cluster solution. However, low-temperature investigations would be necessary to determine the accurate number of Stark levels, as is known from studies on silicate glasses containing erbium with nearly octahedral 6-fold oxygen coordination.[33]

Besides the electron−phonon interaction, the cross-relaxation quenching within Er−O−Er domains, also called clustering in "overdoped" matrix, is another process conserving 1.54 μm fluorescence. This energy-transfer-related deactivation process occurs at critical concentrations near $10^{21}/cm^3$ with distances between Er^{3+} ions approaching 0.5 nm (nearly 5 times the Er^{3+} ion diameter).[32] Accordingly, in our Er^{3+}/ZnO colloids with Er^{3+} concentrations between 10^{20} and $10^{22}/cm^3$ ZnO, one might observe the cross-relaxation quenching when erbium ions increasingly occupy the nanocrystallites.

To find out the aggregation quenching conditions in our experiments, the NIR fluorescence intensity was measured as a function of the number of Er^{3+} ions per ZnO particle. This has been adjusted by varying the Zn content in the Er−O−Zn precursor employed in hydrolysis and condensation (route A) or by varying the ZnO particle concentration used to dissolve a given amount of the erbium acetate salt (route B). Three important results of this study are shown in Figure 5 with the 1.54 μm fluorescence intensity plotted against the number of Er^{3+} ions per ZnO particle.

First, the highest fluorescence intensity has been measured in samples containing around 2 at. % Er. With increasing erbium concentrations on ZnO carriers, the NIR fluorescence intensity drops and approaches a plateau around 20 at. % (with respect to zinc) for both particle sizes.

Second, co-condensed Er^{3+}/ZnO colloids with 3.5 nm particles fluoresce not as strongly as samples with erbium salts being dissolved in ZnO colloids composed of 5 nm crystallites. Refluxed co-condensed sols with 5 nm ZnO/Er^{3+} particles showed the same fluorescence intensity as the colloids with 3.5 nm ZnO/Er^{3+} particles. Hence, the dissolution route produces samples with a lower extent of clustering, and at low Er^{3+} concentrations (20−200 Er^{3+} per ZnO particle), larger crystallites are more appropriate carriers than smaller ones.

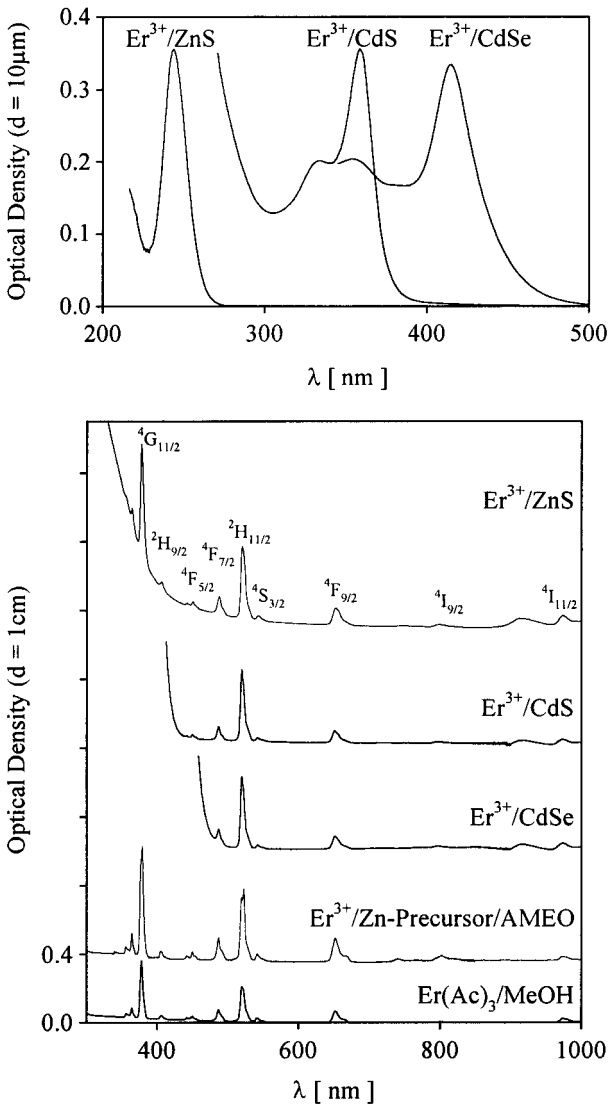

Figure 6. Optical absorption spectra of three ethanolic AMEO-stabilized 0.1 M quantum dot colloids containing ZnS, CdS, or CdSe clusters (average cluster size between 1.5 and 2 nm, the molar Cd(Zn):S(Se) ratio is 2) carrying 20 at. % Er^{3+}. (a, top) Taken with a 10 μm cell. (b, bottom) Taken with a 1 cm cell. For comparison, the spectra of methanolic erbium acetate solution and of the AMEO-complexed Er−O−Zn(Cd) precursor before chalcogenolysis are also included.

Third, the extent to which the Er^{3+} aggregation quenching of the 1.54 μm fluorescence takes place is not as strong as the activation achieved. The most remarkable fact is the large uptake capacity of these nanocrystallites, reflected also in the upper scale of Figure 5 (10^{21}−10^{22} Er^{3+}/cm^3 ZnO).

Optical Absorption and NIR Fluorescence of Er^{3+} in ME Cluster Environments (M = Cd, Zn, E = S, Se). In addition to zinc oxide nanocrystals, we tested AMEO-stabilized ZnS, CdS, and CdSe clusters as erbium carriers in ethanol (for synthesis see Experimental Section). Figure 6 shows the optical absorption spectra of highly concentrated ethanolic 0.1 M chalco-

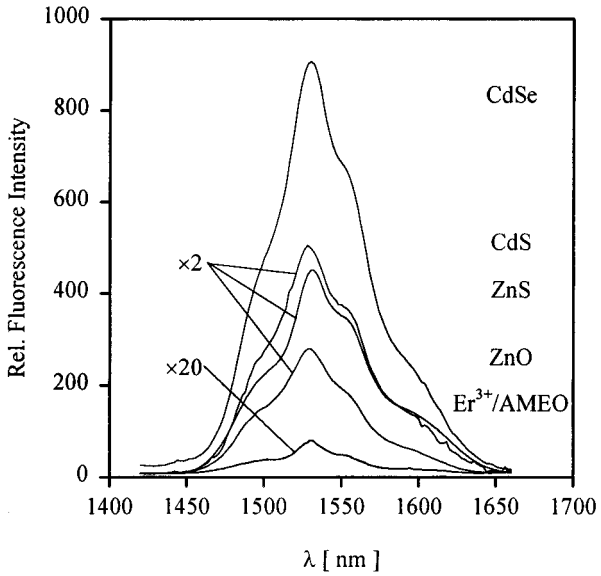

Figure 7. NIR fluorescence of Er^{3+} in AMEO-complexed Zn-(Cd)−O−Er precursor before and after chalcogenolysis in ethanol. For comparison, the ZnO/Er^{3+} spectrum is also included. For fluorescence pumping conditions see Figure 4.

genide cluster solutions with a molar Cd(Zn)/Er^{3+} ratio of 5, taken with a 10 μm cell (part a) and with a 1 cm cuvette (part b). The sharp excitonic transitions at 250 nm for ZnS, 350 nm for CdS, and 410 nm for CdSe reflect the presence of strongly quantized clusters. (ZnS, CdS, and CdSe bulk crystals possess absorption onset at 400, 550, and 700 nm.[1−4]) Their size is approximately 1.6 ± 0.2 nm (nearly 100% surface), which has been determined using HRTEM, SAXS, and XRD methods.[34] It is of note that the presence of Er^{3+} did not affect the cluster nucleation process and their corresponding optical absorption spectra. They exhibit the same shapes as lanthanide-free samples.

The f−f transitions in Er^{3+}, however, undergo similar hyperchromic intensity changes as discussed above for the case of the ZnO carrier (see part b and also Figure 2). Particularly, the hypersensitive $^4G_{11/2}$ and $^2H_{11/2}$ transitions have higher oscillator strength than those of carrier-free systems. Additionally, by comparing the $^2H_{11/2}$ transition of the AMEO-complexed Zn(Cd)/Er precursor before and after the chalcogenolysis (see Figure 6b), the initial pronounced term splitting is suppressed after the chalcogenolysis, without a decrease in oscillator strength. This indicates that the ligand field is dominated by the produced chalcogenide cluster.

The fact that the Er^{3+} ions are trapped in chalcogenide clusters becomes even more evident in Figure 7 displaying the 1.54 μm fluorescence as a function of the cluster environment. For comparison, the data collected on 3.5 nm sized ZnO colloids and carrier-free Er/AMEO complexes in ethanol are also included. Ethanolic AMEO-stabilized Er−Zn(Cd)S cluster solutions are fluorescing 200 times more strongly than ethanolic AMEO−Er complexes and approximately 2 times more intense than Er−ZnO colloids. The highest intensity was detected on CdSe cluster environments.

These effects of the cluster environment on the 1.54 μm fluorescence intensity can be explained in terms of different energies of the optical phonons produced by cluster vibrations. From resonant Raman scattering studies, it is well-known[35] that both CdSe bulk crystals and CdSe quantum dots produce LO phonons with energies of about 200 cm^{-1}, which is lower than in metal sulfides or ZnO (300 cm^{-1} in CdS and 500 cm^{-1} in ZnO). Thus, according to formulas 1−3, the number of phonons needed to conserve the 1.54 μm fluorescence (4f electron LO phonon coupling) is larger in CdSe than in CdS or ZnO, which might explain the highest fluorescence intensity in the case of CdSe.

Furthermore, besides this phonon energy-based correlation of the experimental data, two general questions arise: (1) What is the exact structure and chemical composition of these extremely small chalcogenide clusters activating the 1.54 μm fluorescence? (2) What is the nucleation mechanism of the metal chalcogenide clusters, not influenced by erbium concentrations as high as 20 at. %? In the next section, we give some preliminary explanations based on fractal cluster hypothesis, addressed in detail in ref 34.

Remarks to Structure and Chemistry of II−VI Semiconductor Cluster Carriers and Their Precursors. In our recent synthesis studies we performed a careful chemical analysis of tributylphospine (TBP)-capped CdSe clusters exhibiting the same excitonic feature at 420 nm as the AMEO-stabilized samples employed in the above-described experiments. Both cluster solutions were prepared under identical molecular precursor conditions. From the analysis data we derived a formula $[Cd_{34}Se_{19}(OAc)_{25}(OH)_5(TBP)_{7.5}]$ reflecting the presence of acetates and OH groups in addition to TBP ligands which also has been corroborated in FTIR measurements. It appears that the OH groups serve as bridging ligands between the clusters and erbium. This is supported by the fact that erbium acetate powder readily dissolves in these ethanolic colloidal solutions whereas it does not dissolve in ethanol. Additionally, the use of other precursors such as cadmium or zinc chlorides did not allow synthesis of stable alcoholic colloids.

The presence of hydroxyl and acetate groups after the chalcogenolysis is intimately related to the structure of the Cd(Zn) precursor produced by refluxing ethanolic metal acetate solution prior to complexation with AMEO or TBP and a subsequent hydrolysis or chalcogenolysis. The boiling procedure produces oligomeric acetate-capped metal oxo-ethoxide clusters of the general formula $[M_{10}O_4(OAc)_{12}]$, associated with two water molecules and 10 ethanol ligands, derived from chemical analysis and FTIR data. Hence, it can be easily realized that the above-employed cluster environments are actually oxo-chalcogenides with strongly bound acetate ligands. However, it is still difficult to understand the above-presented dramatic 1.54 μm fluorescence activation in terms of the L_{5-7}−Er−O−Cd(Zn) cluster sequences with L dominated by ethanol and/or (aminopropyl)silane ligands of the surrounding liquid environment.

More realistic seems an assumption of erbium ions being trapped inside of these 1.6 nm sulfide and selenide clusters. SAXS studies on 1.6 nm CdSe cluster solutions proved that these clusters could be mass fractals with the fractal dimension 2, suggesting a structure based on a Koch pyramid.[34]

Figure 8 illustrates the growth of this self-similar cagelike tetrahedral object (also called a 3D Sierpinski

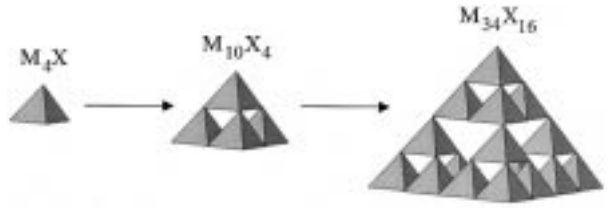

Figure 8. Fractal growth of a regular Koch pyramidal cluster (fractal dimension 2) to its third level and the corresponding stoichiometries assuming M_4X as the initiator with M = Cd, Zn and X = O, S, Se (adapted from ref 34).

triangle) with vertex-shared tetrahedra. The corresponding stoichiometries are also included. The generator of this growth is represented by a collection of four primary M_4X clusters, where X (= O, S, Se) is located within a M_4 tetrahedra (M = Zn, Cd). Applied to CdSe, this initiator is stepwise doubling its size (defined by the Cd−Cd distance of about 0.42 nm in sphalerite) by the transition to the second $M_{10}X_4$ level (0.84 nm) and further to the third level ascribed to a $M_{34}X_{16}$ pyramid (1.68 nm).

Interestingly, the $[M_{10}O_4(OAc)_{12}]$ precursors and the second-level pyramid exhibit the same cluster core stoichiometry, and so do the $[Cd_{34}Se_{19}(OAc)_{25}(OH)_5(TBP)_{7.5}]$ clusters and the third-level $M_{34}X_{16}$ pyramid. In our preliminary theoretical investigations we have found that an Er^{3+} ion, if trapped in the center inside the third-level $Cd_{34}Se_{16}$ pyramid, is exposed to 12 nearest Cd neighbors (cuboctahedron cage) at a distance of about 0.432 nm. The theoretical Er−Cd distance in Er−O−Cd has been calculated to be 0.37 nm (at an angle of 109°). Thus, Er^{3+} would fit fairly well into these cages offering up to 12 coordination sites.

Additional structural analyses (e.g., ESR, EXAFS, SAXS) are required to determine definitely the position of erbium ions in these clusters. Our highly concentrated colloids, optimized for film formation technologies, undergo gelation rather than crystallization. It might be possible, however, to grow large crystals for X-ray crystallographic analysis by replacing the AMEO ligands against more suitable groups.

Conclusions

The strong activation of the 1.54 μm fluorescence of Er^{3+} has been achieved employing II−VI semiconductor quantum dot environments. Up to 20 at. % Er^{3+} could be incorporated into the 1.5−2 nm metal oxo-chalcogenide clusters or slightly larger 3−5 nm ZnO nanocrystals, with the aid of the Cd(Zn)−O groups serving as bridging ligands. Both the electron−phonon interaction and the concentration quenching can be controlled in these new oxo-chalcogenide cluster materials. Additionally, the Koch pyramid hypothesis, supported by synchrotron SAXS and XRD studies,[34] can best explain the above-achieved fluorescence activation as well as the hyperchromic term splitting of the f−f transitions, and vice versa.

The sol−gel-derived II−VI semiconductor cluster concept for incorporation of Er^{3+} extends the range of materials represented by III−V semiconductors, implanted oxygenated Si wafers, and codoped silicate, phosphate, as well as low phonon heavy metal fluoride glasses. However, the above steady-state optical absorption and fluorescence study does not present the final optimized materials applicable for NIR lasing components. The latter requires long fluorescence lifetimes and low damping losses of thick 5−10 μm films produced from the cluster solutions. At present, we are engaged in time-resolved NIR fluorescence studies which is the subject of our next report.[36]

Acknowledgment. This work was supported by the Siemens AG (BMBF project 03N1007C9). We thank Mr. H. Schmidt for his assistance in the laboratory. The authors would like to thank Dr. M. Lerch (Universität Würzburg), Dr. H. W. Schneider, and Dr. H. Albrecht (Siemens AG) for fruitful discussions.

CM9702169